ISSN 1070-3284, Russian Journal of Coordination Chemistry, 2024, Vol. 50, No. 4, pp. 239–245. © Pleiades Publishing, Ltd., 2024.

Synthesis and Study of Mono(arylhydrazino)acenaphthenones and Nickel Complex Based on Pyridine-Substituted Derivative

I. V. Bakaev[a], V. I. Komlyagina[a, b], N. F. Romashev[a, *], and A. L. Gushchin[a]

[a] *Nikolaev Institute of Inorganic Chemistry, Siberian Branch, Russian Academy of Sciences, Novosibirsk, 630090 Russia*

[b] *National Research Novosibirsk State University, Novosibirsk, 630090 Russia*

**e-mail: nikolaj.romashev75@gmail.com*

Received October 20, 2023; revised December 11, 2023; accepted December 29, 2023

Abstract—Three mono(arylhydrazino)acenaphthenones, that is, mono(2-pyridylhydrazino)acenaphthenone (Py-mhan, L^1), mono(4-cyanophenylhydrazino)acenaphthenone (4-CN-Ph-mhan, L^2), and mono(3,4,6-trifluoro-2-pyridylhydrazino)acenaphthenone (^{F}Py-mhan, L^3), were synthesized by the reaction of acenaphthene quinone with the appropriate arylhydrazine salt; compounds L^2 and L^3 were obtained for the first time. The subsequent reaction of L^1 with nickel chloride in 2 : 1 ratio led to the octahedral complex [Ni(Py-mhan)$_2$] (**I**), in which Py-mhan acts as a tridentate ligand. All of the prepared compounds were characterized by elemental analysis, IR and ^{1}H NMR spectroscopy, and cyclic voltammetry; the crystal structures of L^3 and **I** were determined by X-ray diffraction.

Keywords: acenaphthene hydrazones, ligands, X-ray diffraction analysis, complexes, synthesis, nickel, cyclic voltammetry

DOI: 10.1134/S1070328423601644

INTRODUCTION

Mono(arylhydrazino)acenaphthenones (Ar-mhan) are related to the well-known class of imino acenaphthenes [1–5]. A key feature of imino acenaphthenes is the ability to reversibly accept up to four electrons [6–8] and reversibly exchange the electrons with the coordinating metal, which may trigger redox reactions. Therefore, metal complexes based on imino acenaphthenes proved to be effective catalysts for activation of small molecules [9, 10], polymerization of olefins [11–15], hydroamination and hydrosilylation [16–20], and many other reactions [9, 21–23].

A key distinction of Ar-mhan from imino acenaphthenes is the presence of acid NH-proton, the elimination of which gives a resonance-stabilized anion capable of efficient coordination of metal ions in the bidentate fashion. Ar-mhan are also redox-active compounds, which were shown previously to undergo reversible single-electron reduction and irreversible oxidation [24]. However, metal complexes with Ar-mhan virtually have not been studied. Currently, only a few examples of compounds with 3*d* metals (Zn, Co, Cu) obtained by Prof. J. Yang's group are known [25–27]. Our research team synthesized heteroleptic palladium complexes described as [Pd(Ar-bian)(Ar-mhan)]$(CF_3SO_3)_2$, which show intramolecular charge transfer from Ar-mhan to Ar-bian in the near-IR region [24]. The small HOMO–LUMO gap, characteristic of both acenaphthene hydrazones and their complexes suggests that they may be applicable as electron donors for organic solar elements [24, 28].

The purpose of this study was to develop approaches to the synthesis of mono(arylhydrazino)acenaphthenones (Ar-mhan) with electron-withdrawing aromatic substituents and study the coordination of Py-mhan to the Ni(II) ion and electrochemical properties of the obtained compounds.

EXPERIMENTAL

The following commercial chemicals were used as received: acenaphthene quinone (Sigma Aldrich, 99%), $NiCl_2 \cdot 6H_2O$ (Sigma Aldrich, 99%) 4-cyanophenylhydrazine (Sigma Aldrich, 98%), 2-pyridylhydrazine (Sigma Aldrich, 98%), 3,4,6-trifluoro-2-pyridylhydrazine (Sigma Aldrich, 98%). The solvents were purified by standard procedures. Infrared spectra in the 4000–400 cm^{-1} range were measured on a Scimitar FTS 2000 spectrometer using samples as KBr pellets. Elemental analysis for C, H, N, S was performed on a Euro EA 3000 instrument. NMR spectra were run on a Bruker Avance 500 spectrometer at room temperature using internal TMS in $CDCl_3$ as the ^{1}H NMR standard.

Electrochemical measurements for solutions were performed on a 797 VA Computrace instrument (Metrohom, Switzerland) using a 10 mL three-electrode cell. A platinum auxiliary electrode and a silver

Table 1. Main crystallographic data and structure refinement details for L^3 and **I**

Parameter	Value	
	L^3	**I**
Formula	$C_{17}H_8N_3OF_3$	$C_{34}H_{20}N_6O_2Ni$
M	327.26	603.27
Temperature, K	150	150
System	Monoclinic	Monoclinic
Space group, *Z*	$P2_1/n$, 4	$P2_1/n$, 4
a, Å	6.7344(12)	9.2104(7)
b, Å	13.667(2)	18.0055(14)
c, Å	15.240(3)	16.1540(14)
β, deg	95.896(8)	92.452(3)
V, Å^3	1395.3(4)	2676.5(4)
ρ(calcd), g/cm^3	1.558	1.497
μ, mm^{-1}	0.128	0.771
Crystal size, mm	0.210 × 0.025 × 0.012	0.060 × 0.040 × 0.010
Data collection range of θ, deg	2.006–25.451	1.694–25.400
Ranges of *h*, *k*, *l*	$-8 \le h \le 8$, $-15 \le k \le 16$, $-18 \le l \le 16$	$-11 \le h \le 10$, $-21 \le k \le 21$, $-19 \le l \le 19$
Number of measured reflections	11876	25267
Number of unique reflections (R_{int})	2568 (0.0509)	4907 (0.0604)
GOOF	1.044	1.015
R_1/wR_2 (for reflections with $I > 2\sigma(I)$)	0.0510/0.1302	0.0367/0.0791
R_1/wR_2 (for all reflections)	0.0900/0.1470	0.0593/0.0874
$\Delta\rho_{max}$, $\Delta\rho_{min}$, e/Å^3	0.333, –0.209	0.388, –0.382

chloride reference electrode filled with KCl (3 M) were used. A glassy carbon disk (d = 3 mm) was used as the working electrode. A 0.1 M Bu_4NPF_6 solution in dichloromethane served as a supporting electrolyte (scan rate of 100 mV/s). Ferrocene with the potential $E_{1/2}$ = 0.49 V (vs. Ag/AgCl) was used as an internal standard. The concentration was varied in the range from 8×10^{-4} to 2×10^{-3} mol/L. The half-wave potentials ($E_{1/2}$) were calculated as the half-sum of potentials of anodic and cathodic peaks.

X-ray diffraction analysis of compounds L^3 and **I** was performed on a Bruker D8 Venture single-crystal diffractometer (0.5° ω- and φ-scan mode, three-circle goniometer with fixed χ, PHOTON III CMOS detector, focusing with Montel mirrors) at a temperature of 150 K, using MoK_α radiation (λ = 0.71073 Å). The structures were solved using the SHELXT program [29] and refined with the SHELXL program [30] using the ShelXle graphical shell [31]. The hydrogen atoms were located geometrically and refined in the riding model. The X-ray diffraction experiment details are summarized in Table 1.

The full tables of interatomic distances and bond angles, atomic coordinates, and atomic displacement parameters were deposited with the Cambridge Crystallographic Data Centre (CCDC nos. 2301857 (L^3) and 2301856 (**I**), http://www.ccdc.cam.ac.uk/conts/retrieving).

Synthesis of Py-mhan (L^1). A mixture of 2-$PyNHNH_2$ (300 mg, 2.75 mmol) and acenaphthen-

equinone (500 mg, 2.75 mmol) in ethanol (30 mL) was stirred for 3 h. The reaction gave a bright orange precipitate, which was collected on a filter, washed with ethanol, and dried in vacuo. The yield of L^1 was 639 mg (85%).

^{1}H NMR ($CDCl_3$; δ, ppm): 13.12 (s, H_1), 8.35 (d, H_9, J = 4.7 Hz), 8.17 (d, H_2, J = 8.3 Hz), 8.09 (d, H_7, J = 7.0 Hz), 7.91 (t, 2H (H_3, H_6)), 7.80– 7.70 (m, 4H (H_4, H_5, H_{11}, H_{12})), 7.00 (m, H_{10}).

IR (KBr; ν, cm^{-1}): 3468 br.m, 3248 br.m, 3052 br.m, 1676 s, 1607 s, 1593 s, 1573 s, 1553 s, 1502 s, 1458 w, 1437, 1354 w, 130 m, 1252 r, 1190 s, 1148 m, 1057 s, 1026 s, 1007 m, 937 s, 867 m, 831 s, 804 s, 775 s, 746 m, 690 w, 642 s, 582 m, 529 s, 490 w, 455 m, 409 w.

For $C_{17}H_{11}N_3O$

Anal. calcd., %	C, 74.71	H, 4.06	N, 15.38
Found, %	C, 74.4	H, 4.24	N, 15.5

Synthesis of 4-CN-Ph-mhan (L^2). A mixture of 4-cyanophenylhydrazine chloride (466 mg, 2.75 mmol) and acenaphthenequinone (500 mg, 2.75 mmol) in ethanol (30 mL) was stirred for 1.5 h. The reaction yielded a voluminous bright yellow precipitate, which was collected on a filter, washed with ethanol, and dried in vacuo. The yield of L^2 was 713 mg (87%).

^{1}H NMR ($CDCl_3$; δ, ppm): 13.23 (br.s., H_1), 8.21 (d, H_2, J = 8.2 Hz), 8.09 (d, H_7, J = 7.0 Hz), 7.95 (d, H_4, J = 8.3 Hz), 7.91 (d, H_5, J = 6.9 Hz), 7.80 (t, H_3), 7.75 (t, H_6), 7.68 (d, $H_{9,11}$, J = 8.8 Hz), 7.50 (d, $H_{8,12}$, J = 8.7 Hz).

IR (KBr; ν, cm^{-1}): 3460 br.m, 3215 br.m, 3055 br.m, 2220 s, 1676 s, 1608 s, 1557 s, 1516 s, 1454 w, 1435 w, 1417 w, 1244 s, 1173 s, 1059 s, 1026 s, 1009 m, 943 s, 873 m, 845 m, 825 s, 794 s, 775 s, 677 m, 517 w, 500 w.

For $C_{19}H_{11}N_3O$

Anal. calcd., %	C, 76.76	H, 3.73	N, 14.13
Found, %	C, 76.9	H, 3.55	N, 14.0

Synthesis of ^{F}Py-mhan (L^3). A mixture of 3,4,6-trifluoro-2-pyridylhydrazine (2.75 mmol) and acenaphthenequinone (500 mg, 2.75 mmol) in ethanol (30 mL) was stirred for 3 h. The reaction yielded a bright orange precipitate, which was collected on a filter, washed with ethanol, and dried in vacuo. The yield of L^3 was 791 mg (88%). The single crystals of L^3 suitable for X-ray diffraction were obtained by slow diffusion of diethyl ether vapor into a solution of L^3 in dichloromethane.

^{1}H NMR ($CDCl_3$; δ, ppm): 13.54 (br.s, H_1), 8.22 (d, H_2, J = 8.2 Hz), 8.10 (d, H_7, J = 6.7 Hz), 8.09 (d, H_5, J = 6.7 Hz), 7.98 (d, H_4, J = 8.3 Hz), 7.81 (t, H_3), 7.76 (t, H_6), 7.51 (q, H_{11}).

IR (KBr; ν, cm^{-1}): 3457 br.m, 3234 br.w, 3179 br.w, 3064 br.w, 1677 s, 1637 m, 1606 m, 1556 m, 1523 s, 1461 s, 1443 s, 1353 w, 1279 m, 1209 s, 1198 s, 1177 s, 1057 s, 1029 s, 924 m, 921 m, 830 m, 802 m, 776 s, 764 m, 721 w, 685 w, 660 s, 615 w, 583 w, 551 w, 518 m, 487 w, 466 w, 426 w.

For $C_{17}H_8N_3OF_3$

Anal. calcd., %	C, 62.39	H, 2.46	N, 12.84
Found, %	C, 62.2	H, 2.65	N, 12.6

Synthesis of [Ni(Py-mhan)$_2$] (I). Py-mhan (230 mg, 0.84 mmol) and triethylamine (200 μL) were added to a suspension of $NiCl_2 \cdot 6H_2O$ (100 mg, 0.42 mmol) in ethanol (20 mL). A finely crystalline red precipitate was formed within 2 h. The precipitate was collected on a filter, washed with ethanol, and dried in vacuo. The yield of **I** was 203 mg (80%). The single crystals of **I** suitable for X-ray diffraction were obtained by slow diffusion of diethyl ether vapor into a solution of **I** in dichloromethane.

IR (KBr; ν, cm^{-1}): 3047 w, 3020 w, 1596 s, 1521 s, 1483 w, 1457 m, 1416 s, 1366 w, 1330 m, 1302 m, 1278 m, 1238 s, 1178 s, 1135 s, 1103 m, 1088 m, 1067 m, 1025 m, 1004 m, 974 m, 965 m, 899 s, 874 m, 827 m, 773 s, 747 w, 674 w, 628 w, 590 w, 531 m, 494 w, 422 w.

For $C_{34}H_{20}N_2O_2Ni$

Anal. calcd., %	C, 67.69	H, 3.34	N, 13.93
Found, %	C, 67.4	H, 3.13	N, 13.6

RESULTS AND DISCUSSION

Mono(arylhydrazino)acenaphthenones (Ar-mhan) can be obtained by condensation of acenaphthenequinone with arylhydrazines or their salts in 1 : 1 molar ratio in ethanol or toluene [24]. It is important that this reaction gives only the product of addition of one equivalent of arylhydrazine to acenaphthenequinone. Most likely, this is due to the presence of tautomeric equilibrium between the keto hydrazone and aza enol forms [25].

In this work, three Ar-mhan compounds were obtained: Py-mhan (L^1), 4-CN-Ph-mhan (L^2), and ^{F}Py-mhan (L^3) (Scheme 1). The subsequent reaction of L^1 with $NiCl_2 \cdot 6H_2O$ in the presence of triethylamine affords the complex [Ni(Py-mhan)$_2$] (**I**). The reaction involves elimination of the hydrazine proton of Py-mhan followed by coordination of the Py-mhan anion.

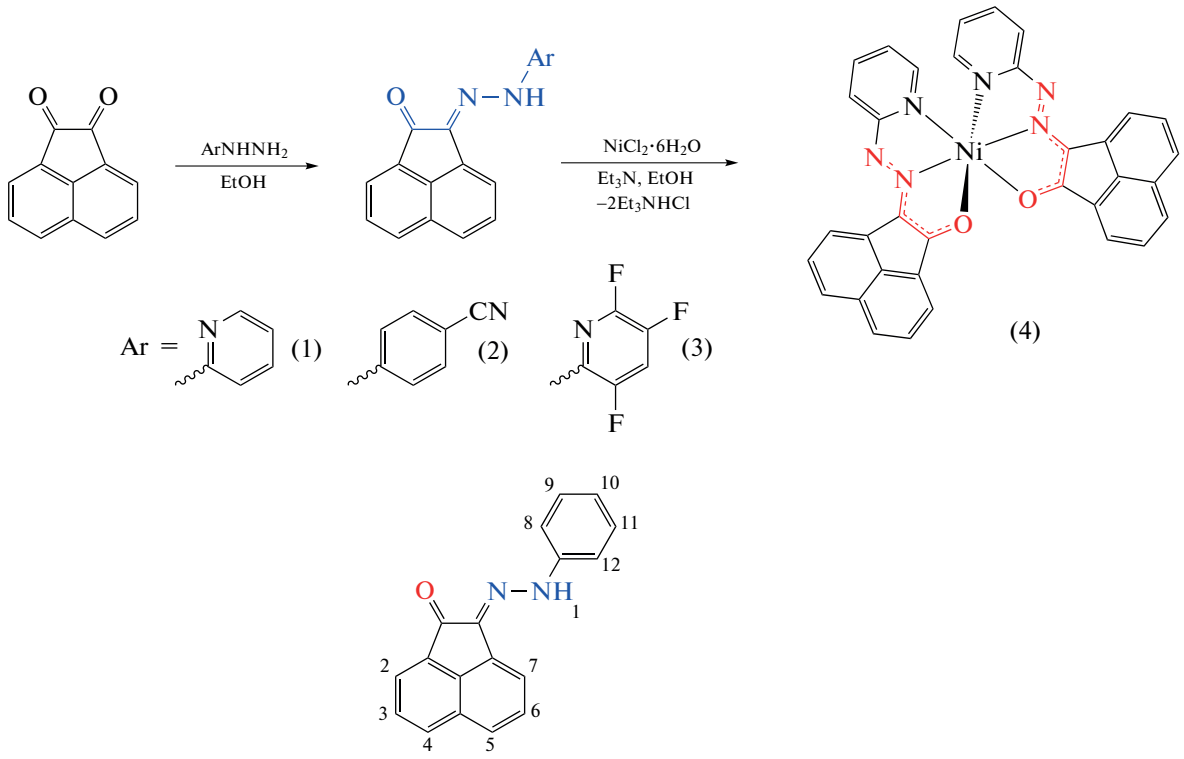

Scheme 1. Synthesis of compounds L^1–L^3 and **I** and proton numbering in compounds L^1–L^3.

The purity of compounds L^1–L^3 and **I** was confirmed by elemental analysis.

The IR spectra of L^1–L^3 exhibit broad ν(N–H) stretching bands in the 3468–3457 cm^{-1} range. The ν(C=O) and ν(C=N) modes occur in the 1677–1676 and 1608–1523 cm^{-1} ranges, respectively. The δ_{oop}(C–H) vibrations of the acenaphthene moiety and the substituted benzene ring occur at 831–775 cm^{-1}. In the IR spectrum of complex **I**, the ν(C=O) (1596 cm^{-1}) and ν(C=N) (1521 cm^{-1}) stretching bands are shifted to lower energy compared to those of the free ligand, indicating coordination of Py-mhan to the nickel ion.

In the ^{1}H NMR spectra of L^1–L^3, the signals of all aromatic and aliphatic protons were detected. The hydrazine proton signals appear as broadened singlets at 13.12, 13.23, and 13.54 ppm for L^1, L^2, and L^3, respectively. The signals of the acenaphthene moiety are manifested as four doublets with the characteristic spin–spin coupling constant $^3J_{HH}$ = 6.7–8.2 Hz and two triplets. For compound **I**, the proximity of proton signals gives rise to a multiplet in the aromatic region. Splitting of the proton signals for the substituted phenyl ring in L^2 and L^3 corresponds to the type of substitution. For complex **I**, it was impossible to record the ^{1}H NMR spectrum because of the presence of paramagnetic Ni(II) center.

The molecular structure of compounds L^3 and **I** was established by X-ray diffraction. The single crystals of L^3 were obtained by slow diffusion of diethyl ether vapor into a solution of L^3 in dichloromethane. The structure of L^3 is shown in Fig. 1. The C–O and C–N distances are 1.238(3) and 1.302(3) Å, respectively, which is somewhat longer than the standard lengths of the C=O and C=N bonds. Meanwhile, the C–C and N–N distances are somewhat shortened, being 1.498(4) and 1.341(3) Å, respectively; this is slightly shorter than the standard C–C and N–N single bond lengths. This may be due to the presence of ketohydrazone and azaenol tautomeric forms, which differ from each other in the bond lengths and hydrogen atom positions, resulting in the averaging of bond lengths in the molecule [25]. The O···H hydrogen bond closes a six-membered ring, with the O–N distance being 2.718(3) Å.

The single crystals of **I** were obtained by slow diffusion of diethyl ether vapor into a solution of **I** in dichloromethane. The molecular structure of **I** is presented in Fig. 2; characteristic bond lengths are summarized in Table 2. The nickel atom occurs in a distorted octahedral environment consisting of four nitrogen atoms and two oxygen atoms. Each ligand is coordinated as an anion in the tridentate fashion by the nitrogen and oxygen atoms of the ketohydrazone moiety and the nitrogen atom of the pyridine ring. The Ni–N(Py) distances are equal to within the error of measurement, being 2.061(2) and 2.058(2) Å, which falls in the range of Ni–N bond lengths with pyridine ligands [32–35]. The Ni–N (hydrazone) distances are

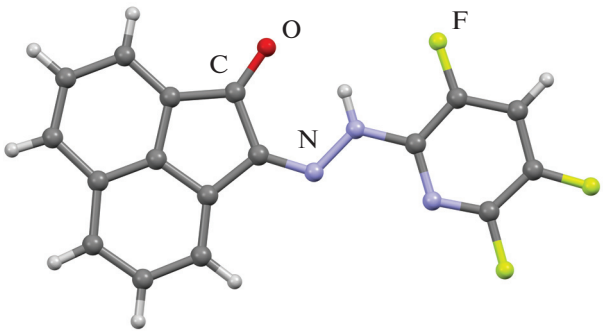

Fig. 1. Molecular structure of L^3 according to X-ray diffraction data.

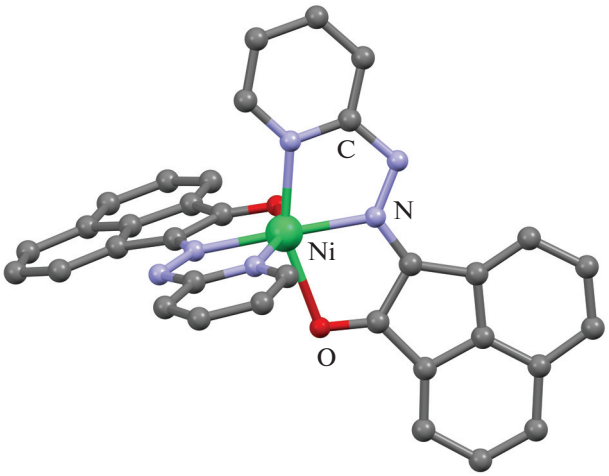

Fig. 2. Molecular structure of **I** according to X-ray diffraction data.

also equal and amount to 1.997(2) and 1.996(2) Å, while the Ni–O distances are 2.1767(18) and 2.2461(17) Å. The C–N, C–O, and N–N distances in the ketohydrazone moiety of Py-mhan correspond to bond order of 1.5, which is attributable to the resonance delocalization of negative charge over the ketohydrazone moiety, stabilizing this anion.

Like related imino acenaphthenes, mono(arylhydrazino)acenaphthenones are redox-active compounds that can add electrons owing to the ketoimine moiety. Their main difference from imino acenaphthenes is that they can be oxidized to form a phenoxyl radical [36].

The redox properties of the compounds were studied by cyclic voltammetry (CV). The main electrochemical characteristics are summarized in Table 3. The CV curves of L^1–L^3 (Fig. 3) exhibit two main peaks: an anodic peak at 1.27 to 1.70 V (vs. Ag/AgCl) corresponding to oxidation and a cathodic peak accompanied by an anodic counter-peak with $E_{1/2}$ from –1.11 to –1.19 V corresponding to reduction. For compounds L^2 and L^3, the $|I_a/I_c|$ current ratio markedly differs from unity; hence, the reduction processes should be described as quasi-reversible. The peaks detected in CV curves can be interpreted in the following way. The cathodic peak is responsible for the quasi-reversible single-electron reduction of the ketohydrazone moiety of Ar-mhan, resulting in the generation of a radical anion relatively stable throughout the CV experiment. No further Ar-mhan reduction was observed down to –2.00 V (vs. Ag/AgCl). The anodic peak corresponds to irreversible oxidation to give an unstable radical cation, the deprotonation of which affords the phenoxyl radical (Scheme 2) [36]. Also, additional cathodic and anodic peaks are observed in the region from –0.50 to 0.12 V; they disappear if only cathodic or only anodic potential sweep is performed. Thus, these peaks may be due to by-products formed in the chemical transformations that follow the electron transfer.

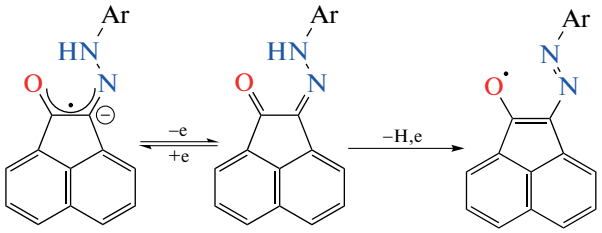

Scheme 2. Redox reactions of Ar-mhan.

Mention should be made of the influence of substituents in the Ar-mhan aromatic ring on the redox potentials: increase in the electron-withdrawing properties of substituents (from L^1 to L^3) is accompanied by a noticeable shift of the oxidation potential to the anodic region. The reduction potential changes insignificantly.

The CV curves of complex **I** exhibit quite a few peaks (Fig. 4). Two quasi-reversible reduction peaks are observed in the cathodic region at $E_{1/2} = -1.09$ and –1.37 V (vs. Ag/AgCl). In the anodic region, there are two irreversible oxidation peaks at 1.08 and 1.21 V. The cathodic processes can be classified as the single-elec-

Table 2. Selected geometric parameters of the molecular structure of **I**

Bond	Bond length, Å
Ni–N (Py)	2.061(2)/2.058(2)
Ni–N (hydrazone)	1.997(2)/1.996(2)
Ni–O	2.1767(18)/2.2461(17)
C–O	1.253(3)/1.248(3)
C–C	1.452(3)/1.452(3)
C–N	1.319(3)/1.317(3)
N–N	1.317(3)/1.315(3)

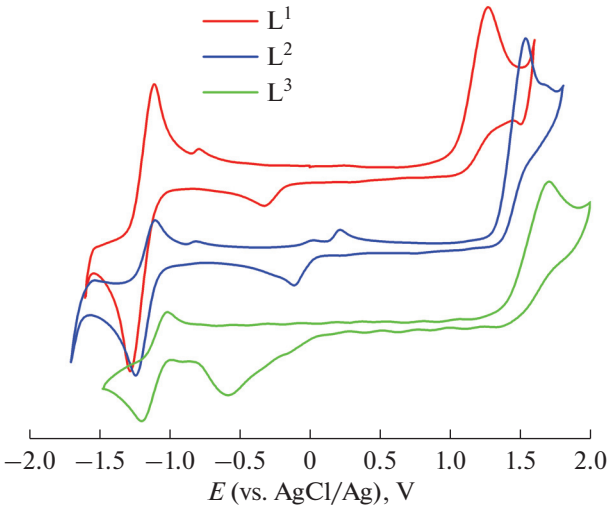

Fig. 3. CV curves of compounds L^1–L^3 in the potential range from −1.6 to 1.7 V (for L^1); −1.75 to 1.8 V (for L^2);−1.5 to 2.0 V (for L^3) (CH_2Cl_2, GC electrode, $c(L^1–L^3) = 8 \times 10^{-4}–2 \times 10^{-3}$ M, v = 100 mV/s, 0.1 M of $^nBu_4NPF_6$, vs. Ag/AgCl).

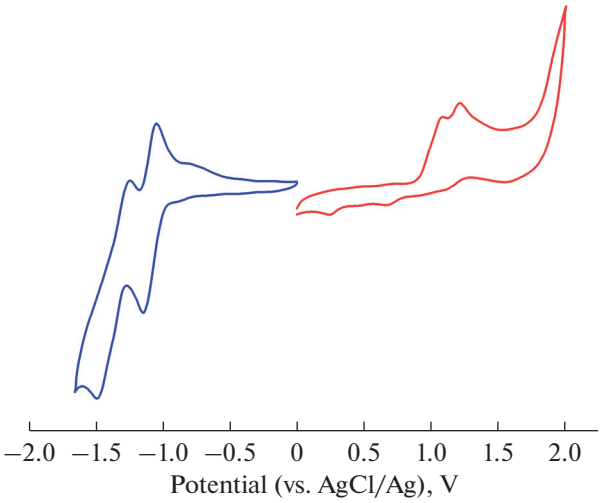

Fig. 4. CV curves of compound **I** in the potential range from 0 to −1.7 V and from 0 to 2.0 V (CH_2Cl_2, GC electrode, $c(L^1–L^3) = 1 \times 10^{-3}$ mol/L, v = 100 mV/s, 0.1 mol/L of $^nBu_4NPF_6$, vs. Ag/AgCl).

tron reduction of each ketohydrazone moiety of Armhan, in view of the similarity of the reduction potentials for L^1 and **I**. A previous study reports the ligand-centered two-electron reduction of a related complex, $[Ni(PAPL)_2]$ (PAPL = 1-(2-pyridylazo)-2-phenanthrole), at −1.0 and −1.3 V (vs. Ag/AgCl) [36]. The participation of nickel in these processes cannot be ruled out either. For the structurally similar $[Ni(Phen\text{-}bian)_2]$ complex, which shows two reversible reduction waves at −1.21 and −1.61 V (vs. Fc^+/Fc), the authors suggested Ni^{II}/Ni^{I} and Ni^{I}/Ni^{0} metal-centered redox transitions [37]. The anodic peaks appear to be related to the oxidation of each Armhan to a phenoxyl radical.

Thus, we obtained a series of new mono(arylhydrazino)acenaphthenones L^1–L^3 containing electron-withdrawing aryl substituents of different nature and the first example of nickel complex **I** based on mono(arylhydrazino)acenaphthenone L^1 and characterized the compounds by a set of physicochemical methods, including X-ray diffraction analysis. Compounds L^1–L^3 and **I** can be both reduced and oxidized over a broad range of potentials from −1.4 to 1.7 V; the reduction processes are quasi-reversible, while oxidation processes are irreversible and are accompanied by structural rearrangement.

Table 3. Redox potentials for compounds L^1–L^3 and **I***

Compound	$E_{1/2}$, V	I_a/I_c	E_a, V
L^1	−1.19	0.92	1.27
L^2	−1.17	0.50	1.54
L^3	−1.11	0.63	1.70
I	−1.09, −1.37	0.66, 0.56	1.08, 1.21

* CV (CH_2Cl_2, GC electrode, c(L^1–L^3 and **I**) = $8 \times 10^{-4}–2 \times 10^{-3}$ mol/L, v = 100 mV/s, 0.1 mol/L of $^nBu_4NPF_6$, vs. Ag/AgCl).

ACKNOWLEDGEMENTS

The authors are grateful to the Ministry of Science and Higher Education of the Russian Federation and the Collective Use Center of the Nikolaev Institute of Inorganic Chemistry, Siberian Branch, Russian Academy of Sciences.

FUNDING

This study was supported by the Russian Science Foundation (grant no. 23-23-10062) and the Government of the Novosibirsk Region.

CONFLICT OF INTEREST

The authors of this work declare that they have no conflicts of interest.

REFERENCES

1. Wang, J., Soo, H.Sen, and Garcia, F., *Commun. Chem.*, 2020, vol. 3, no. 1, p. 133.
2. Fomenko, I.S. and Gushchin, A.L., *Russ. Chem. Rev.*, 2020, vol. 89, no. 9, p. 966.
3. Komlyagina, V.I., Romashev, N.F., Besprozvannykh, V.K., et al., *Inorg. Chem.*, 2023, vol. 62, no. 29, p. 11541.
4. Romashev, N.F., Mirzaeva, I.V., Bakaev, I.V., et al., *J. Struct. Chem.*, 2022, vol. 63, no. 2, p. 242.
5. Romashev, NF., Bakaev, I.V., Komlyagina, V.I., et al., *J. Struct. Chem.*, 2022, vol. 63, no. 8, p. 1304.

6. Fedushkin, I.L., Skatova, A.A., Chudakova, V.A., and Fukin, G.K., *Angew. Chem., Int. Ed. Engl.*, 2003, vol. 42, no. 28, p. 3294.
7. Fedushkin, I.L., Maslova, O.V., Baranov, E.V., and Shavyrin, A.S., *Inorg. Chem.*, 2009, vol. 48, no. 6, p. 2355.
8. Bendix, J. and Clark, K.M., *Angew. Chem., Int. Ed. Engl.*, 2016, vol. 55, no. 8, p. 2748.
9. Bernauer, J., Pölker, J., and Jacobi von Wangelin, A., *ChemCatChem*, 2022, vol. 14, no. 1, p. e202101182.
10. Chacon-Teran, M.A. and Findlater, M., *Eur. J. Inorg. Chem.*, 2022, vol. 2022, no. 30, p. e202200363.
11. Johnson, L.K., Killian, C.M., and Brookhart, M., *J. Am. Chem. Soc.*, 1995, vol. 117, no. 23, p. 641415.
12. Leatherman, M.D., Svejda, S.A., Johnson, L.K., and Brookhart, M., *J. Am. Chem. Soc.*, 2003, vol. 125, no. 10, p. 3068.
13. Bridges, C.R., McCormick, T.M., Gibson, G.L., et al., *J. Am. Chem. Soc.*, 2013, vol. 135, no. 35, p. 13212.
14. Zhai, F. and Jordan, R.F., *Organometallics*, 2017, vol. 36, no. 15, p. 2784.
15. Wu, R., Klingler, W., Stieglitz, L., et al., *Coord. Chem. Rev.*, 2023, vol. 474, no. 1, p. 214844.
16. Fedushkin, I.L., Nikipelov, A.S., Morozov, A.G., et al., *Chem.-Eur. J.*, 2012, vol. 18, no. 1, p. 255.
17. Yakub, A.M., Moskalev, M.V., Bazyakina, N.L., and Fedushkin, I.L., *Russ. Chem. Bull.*, 2018, vol. 67, no. 3, p. 473.
18. Arrowsmith, M., Hill, M.S., and Kociok-Kohn, G., *Organometallics*, 2011, vol. 30, no. 6, p. 1291.
19. Saini, A., Smith, C.R., Wekesa, F.S., et al., *Org. Biomol. Chem.*, 2018, vol. 16, no. 48, p. 9368.
20. Tamang, S.R., Cozzolino, A.F., and Findlater, M., *Org. Biomol. Chem.*, 2019, vol. 17, no. 7, p. 1834.
21. Gushchin, A.L., Romashev, N.F., Shmakova, A.A., et al., *Mendeleev Commun.*, 2020, vol. 30, no. 1, p. 81.
22. Fomenko, I.S., Gongola, M.I., Shul'pina, L.S., et al., *Catalysts*, 2022, vol. 12, no. 10, p. 1168.
23. Romashev, N.F., Bakaev, I.V., Komlyagina, V.I., et al., *Int. J. Mol. Sci.*, 2023, vol. 24, no. 13, p. 10457.
24. Bakaev, I.V., Romashev, N.F., Komlyagina, V.I., et al., *New J. Chem.*, 2023, vol. 47, no. 40, p. 18825.
25. Zhou, J.L., Xu, Y.H., Jin, X.X., et al., *Inorg. Chem. Commun.*, 2016, vol. 64, p. 67.
26. Zhou, J.L., Sun, H.W., Yin, D.H., et al., *J. Mol. Struct.*, 2017, vol. 1134, p. 63.
27. Gao, Q., Song, Y., Zheng, C., et al., *J. Mol. Struct.*, 2020, vol. 1214, p. 128228.
28. Su, Y.X., Zhang, C.Z., and Song, M.X., *Acta Crystallogr., Sect. C: Struct. Chem.*, 2017, vol. 73, no. 6, p. 458.
29. Sheldrick, G.M., *Acta Crystallogr., Sect. A: Cryst. Adv.*, 2015, vol. 71, no. 1, p. 3.
30. Sheldrick, G.M., *Acta Crystallogr., Sect. C: Struct. Chem.*, 2015, vol. 71, p. 3.
31. Hübschle, C.B., Sheldrick, G.M., and Dittrich, B., *J. Appl. Crystallogr.*, 2011, vol. 44, no. 6, p. 1281.
32. Soldatov, D.V., *Mendeleev Commun.*, 1997, vol. 7, no. 3, p. 100.
33. Bose, N. and Lynton, H., *Can. J. Chem.*, 1973, vol. 51, no. 12, p. 1952.
34. Zhang, H. and Fang, L., *Acta Crystallogr., Sect. E: Struct. Rep. Online*, 2005, vol. 61, no. 1, p. m1.
35. Wriedt, M., Jess, I., and Näther, C., *Acta Crystallogr., Sect. E: Struct. Rep. Online*, 2010, vol. 66, no. 7, p. m780.
36. Van Damme, N., Lough, A.J., Gorelsky, S.I., and Lemaire, M.T., *Inorg. Chem.*, 2013, vol. 52, no. 22, p. 13021.
37. Niklas, J.E., Farnum, B.H., Gorden, J.D., and Gorden, A.E.V., *Organometallics*, 2017, vol. 36, no. 23, p. 4626.

Translated by Z. Svitanko